Physica C: Superconductivity and its applications 639 (2025) 1354813

Contents lists available at ScienceDirect

Physica C: Superconductivity and its applications

journal homepage: www.elsevier.com/locate/physc

Heat capacity and magnetic properties of NbTiN films in the bulk limit

Elena Cimpoiasu [a,*], Viorel Sandu [b], Karwan Rostem [c], Edward J. Wollack [c], Ari D. Brown [c], Kevin H. Miller [c], Vilem Mikula [c,d]

[a] United States Naval Academy, Annapolis, MD, 21402 USA
[b] National Institute of Materials Physics, Bucharest, Magurele, 077125 Romania
[c] NASA Goddard Space Flight Center, Greenbelt, MD 20771 USA
[d] American University, Washington, District of Columbia, 20016 USA

ARTICLE INFO

Keywords:
NbTiN
Thin films
Superconductor
Heat capacity
Magnetic properties

ABSTRACT

Heat capacity and magnetic measurements were used to extract superconducting parameters for deposited NbTiN films in the bulk limit, including the critical temperature, the ratio of the superconducting gap to the critical temperature, the phase coherence length, and the upper critical field. We found that the film is a strong coupling superconductor, with a small phase coherence length, consistent with trends reported in the literature. Due to the large thickness, these materials correspond to 3D analogues of bulk NbTiN. The upper critical fields determined from heat capacity and magnetic field measurements are different, emphasizing the sensitivity of magnetic field measurements to defects. The Ginzburg number is much smaller compared to high-T_c superconductors, while magnetic relaxation measurements point towards a Kim-Anderson vortex creep regime.

1. Introduction

The ternary compound niobium-titanium-nitride (NbTiN) is a superconductor with a relatively high critical temperature, $T_c \cong 15$ K, which has multiple practical applications, including in field sensing as nanowire-single-photon detectors [1–6], as superconductor-insulator-superconductor mixers [7–11], impedance-matched absorber coatings [12], and superconducting coating cavities and resonators [13–20]. Nanowire single-photon detectors based on NbTiN are characterized by a close-to-unity efficiency [21–23], fast recovery time due to a low kinetic inductance, low timing jitter due to high switching current [23–27], high photon number resolving, and extremely low noise/dark counts [28–32]. NbTiN has a good chemical and physical stability with a reduced amount of nitrogen vacancies [33], the main drawback of niobium nitride that makes it less useful for thin films applications [34, 35]. In addition, the disorder observed in ultra-thin films induces localization of Cooper pairs [36,37]. This renders these materials a valuable candidate for super-insulator applications.

Since the applications of NbTiN, as well as the investigations on the more exotic properties, are related to the transport properties, most studies have been focused on conductivity and current-voltage measurements. Reported investigations focusing on other physical properties are scarce [38]. To close this gap, the aim of this paper is to provide a systematic study of the magnetic and heat capacity properties of NbTiN films of general interest for low temperature applications. These films are thick and their properties are closer to a hypothetic bulk NbTiN with the ratio N/(Nb+Ti) =1. We should also add that thick film properties provide a first order approximation to thin film properties that may be useful for superconducting device design.

2. Experimental methods

A series of NbTiN films were sequentially deposited on undoped cz-Si (001) wafers (ρ =20 Ω−cm). The deposition was performed by co-sputtering Nb (0.9995 purity) and Ti (0.9999 purity) via pulsed DC magnetron sputtering in a nitrogen-rich environment in a stainless steel, ultrahigh vacuum (1×10^{-9} Torr base pressure) chamber at ambient temperature. Rutherford backscattering spectroscopy analysis revealed a $(Nb_{0.63}Ti_{0.37})_{0.50}N_{0.50}$ stoichiometry. Prior to fabrication, both the chamber walls and substrate holder were coated with a NbTiN passivation layer to avoid the possibility of sample contamination by ferromagnetic media. The thickness of the NbTiN layer was 3400 nm. Chips of 0.28 × 0.28 cm^2 with 0.1 mg of NbTiN layer were cut from the wafer for measurements. The corresponding mass density is 3.75 g cm^{-3}. For comparison with other results, data extracted from magneto-conductance measurements yielded a mass density of 3 and 3.6 gcm^{-3}

* Corresponding author.
E-mail address: cimpoias@usna.edu (E. Cimpoiasu).

https://doi.org/10.1016/j.physc.2025.1354813
Received 20 August 2025; Received in revised form 26 September 2025; Accepted 2 November 2025
Available online 3 November 2025
0921-4534/Published by Elsevier B.V.

for films of 6 and 9 nm, respectively [39]. Grazing incidence X-ray diffraction data provided the d-spacings for the thick NbTiN films. Data confirm the cubic structure with an average value of the lattice parameter $a = 0.440 \pm 0.003$ nm. This value is close to $0.435 \leq a \leq 0.441$ nm reported elsewhere for NbTiN films (although with different stoichiometries and deposited on different substrates) [40–42]. However, we cannot exclude a variation of the compositional ratio in the depth of the sample. Such a variation has been seen before by XPS depth profile investigation on NbTiN thin films of different thickness [41]. We also cannot exclude grain boundaries, other defects, or a certain level of disorder. The heat capacity and the magnetic properties were investigated using a Physical Properties Measurement System by Quantum Design platform equipped with the heat capacity, dc/ac susceptibility, and vibrating sample magnetometry options.

3. Results and discussions

3.1. Heat capacity

The temperature T and field B dependence of the heat capacity $C(T, B)$ of the NbTiN film were found by measuring first the heat capacity of the silicon substrate without the film, followed by the measurement of the silicon substrate with the film. The heat capacity of the film was found by subtracting the two signals. Raw data are shown in Fig. 1.

The results for zero magnetic field are displayed in Fig. 2(a) and show the jump typical for the superconducting transition. Although the method is affected by the noise, the data are reasonable and main features can be discerned. The measured heat capacity contains contributions from phononic, electronic, and superconducting degrees of freedom [43,44]. Above the critical temperature T_c, the normal state heat capacity C_n, has two contributions, one from the electronic system, which is linear in temperature, $C_{el}(T) = \gamma T$, and one from the phonons of the lattice, which is cubic in temperature, $C_{ph}(T) = \beta T^3$. Thus, $C_n = \gamma T + \beta T^3$ for the temperature range explored. The Sommerfeld coefficient γ is proportional to the density of states of electrons $N(\varepsilon_F)$ at the Fermi energy ε_F and is usually temperature independent for a normal metal although this may not be the case for compounds with strong electron–phonon coupling [45]. β depends on the Debye temperature θ_D as θ_D^{-3}

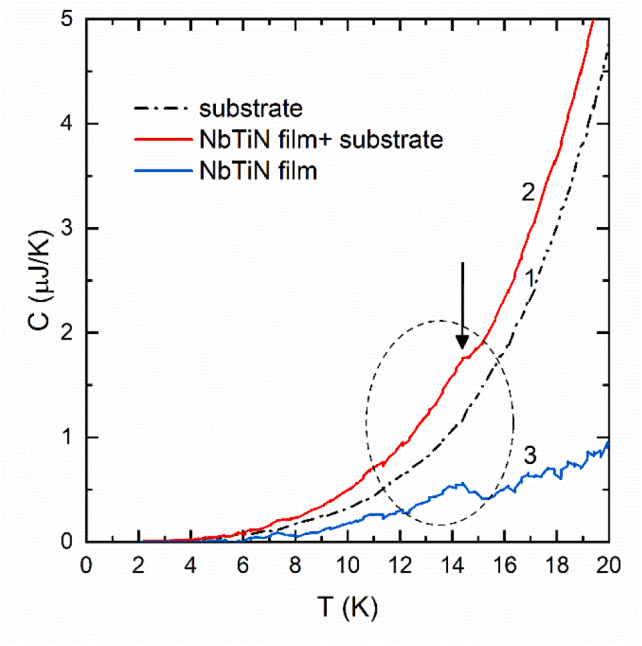

Fig. 1. Raw data of heat capacity measurements of NbTiN film deposited on a Si substrate. The arrow points to the superconducting transition.

and is not expected to change in the superconducting state.

The two contributions can be extracted using the plot of $C(T)/T = \gamma + \beta T^2$ vs T^2 at high temperatures where $C = C_n$. As seen in Fig. 2(b), this plot is linear at temperatures above the superconducting transition. The electronic part of the heat capacity is obtained by subtracting the phononic contribution extrapolated from the normal state above critical temperature $C_{el}(T) = C(T) - \beta T^3$. The electronic heat capacity divided by temperature C_{el}/T versus T is shown in the inset to Fig. 2(b). The critical temperature, recorded at the mid jump, is $T_c = 14.8$ K. Previously it was reported that T_c for a sample with the ratio N/(Nb+Ti) =1 increases slowly above $d = 50$ nm and reaches $T_c = 14.7$ K for $d = 200$ nm [41]. This result is very close to $T_c = 14.83$ K for our films with $d = 3400$ nm and approaching the bulk limit. It is important to note that other thin films we fabricated using a similar method showed a similar T_c, indicating that the critical temperature is not dependent on thickness for our materials.

The extrapolation of the normal state C_{el}/T to $T = 0$ provides the Sommerfeld coefficient.

Data obtained from the linear fit for the normal state yield $\gamma_n = 2.22 \pm 0.22$ mJ mol^{-1} K^{-2} and the Debye temperature, $\theta_D = \left(\frac{12\pi^4 R}{5\beta_n}\right)^{1/3} = 345$ K, with $\gamma_n = \gamma/\nu$, $\beta_n = \beta/\nu$, where ν is the number of moles and $R = 8314$ mJ K^{-1}mol^{-1}, the universal gas constant. The observed value of γ_n is higher than for some pure metals, like Au, Ag, Cu, Al, but smaller than for Zr (3.03 mJ mol^{-1} K^{-2}) or Ir (3.14 mJ mol^{-1} K^{-2}) [46]. A comparison of γ_n with other published results obtained from the photoresponse in the time domain [39,45] for two ultra-thin films of different thicknesses (6 and 9 nm) can be performed assuming $Nb_{0.6}Ti_{0.4}$ N and the mass density provided in the above cited references. For both films, $\gamma_n \approx 1.86$ mJ mol^{-1} K^{-2}, which is smaller than the extracted value for our samples.

For the phononic coefficient, results from Refs. 39 and 47 yield $\beta_n = 0.067$ and 0.158 mJ mol^{-1} K^{-4} for the two films, assuming $C_{ph} \propto T^3$. These values are different than $\beta_n = 0.047$ mJ mol^{-1} K^{-4} for our thick film. This discrepancy might be the result of the fact that, for ultra-thin films, the expected $C_{ph} \propto T^3$ is not obeyed. The interplay between phonon softening due to the strong influence of the surfaces of the film and constituent grains, which increase the phonon heat capacity C_{ph} [48], and the depletion of long wavelength phonon states at low temperatures that occurs when the wavelength of thermal phonons becomes longer than the film thickness [49] might result in a different temperature dependence. Actually, a more recent model suggests that the low-temperature phonon heat capacity C_{ph} for ultra-thin films does not follow the Debye cubic dependence on temperature, but rather $C_{ph} \propto T^4$, due to quantum confinement [50]. This model shows a reduction in C_{ph} with decreasing film thickness associated with the reduction in the density vibrational modes (which store heat as internal energy) at low temperatures. It is worth noting that the model recovers the Debye dependence, $C_{ph} \propto T^3$, as the thickness of the film becomes sufficiently large, like in our case. A similar thickness dependence of γ_n could be inferred if confinement is invoked [51]. Therefore, γ_n for thick films like ours should be larger compared to the value for thin films, as, indeed, our results confirm.

The Debye temperature of 345 K is much higher than the 231 K calculated for the film of 9 nm thickness of Ref 39. Actually, it was found that a reduced thickness of metallic films decreases θ_D as the role of surface phonons become more important [52]. However, 345 K is smaller than the only θ_D values that we found in the literature for $Nb_xTi_{1-x}N$, which would span between 634 K for $x = 0$ and 924 K for $x = 1$ [53]. We should note that the Debye temperatures from Ref. 53 were computed for a putative ideal bulk $Nb_xTi_{1-x}N$ from first principles and not extracted directly from experimental results.

The normalized jump of heat capacity at T_c from the inset of Fig. 2(b) is $\Delta C_{es}/\gamma T_c = 2.19 \pm 0.25$, which is larger than the theoretical value

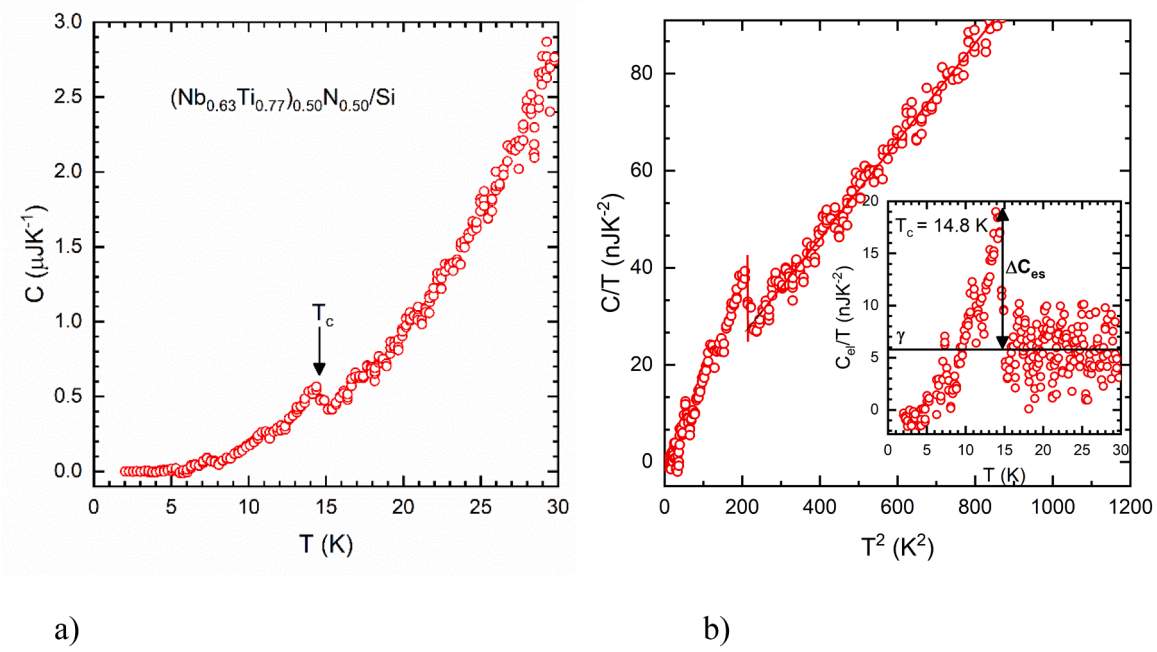

Fig. 2. a). Temperature dependence of NbTiN film on a Si (100) substrate in zero magnetic field. b) Plot of C/T vs. T^2 for the same field. The high temperature line is the fit with the equation $C/T = \gamma + \beta T^2$. Inset: temperature dependence of the electronic heat capacity divided by temperature as obtained after subtraction of the phonon contribution.

$\Delta C_{es}/\gamma T_{c,BCS} = 1.43$ proposed for weak coupling BCS superconductors. Note that similarly high values were reported for Nb_3Sn ($\Delta C_{es}/\gamma T_c = 2.5$ [54]). According to the single-band α-model [55], all thermodynamic quantities, $\Delta C_{es}(T)/\gamma T_c$ included, are scaling functions of the parameter $\alpha \equiv \Delta_g(0)/k_B T_c$, where $\Delta_g(0)$ is the zero-temperature superconducting gap:

$$\Delta C_{es}\Big/\gamma T_c = \Delta C_{es}\Big/\gamma T_{c,BCS}(\alpha/\alpha_{BCS})^2 \quad (1)$$

with $\alpha_{BCS} \approx 1.764$. Consequently, Eq. 1 yields $\Delta_g(0)/k_B T_c = 2.18 \pm 0.27$ for the samples reported here. This result confirms that our material is a strong coupling superconductor. The temperature dependence of measured $C_{es}(T)/\gamma T_c$, together with the calculated values for $\alpha = 2.18$ and the universal $\alpha_{BCS} = 1.764$ are shown in Fig. 3. The temperature dependence of the curve with $\alpha = 2.18$ was obtained by the interpolation of data from Ref [55].

For comparison, terahertz time-domain transmission spectroscopy measurements found $\Delta_g(0)/k_B T_c = 1.86$ for a 280 nm film of $Nb_{0.5}Ti_{0.5}N_{0.28}$ [56], 2.0 for a thick film, and 2.55 for a mesh-shaped film, respectively [57]. Moreover, tunneling spectroscopy data on $Nb_{0.8}Ti_{0.2}N$ thin films found $\Delta_g(0)/k_B T_c = 2.05$ [58] but in the presence of several weaker gaps, indicative of a multiphase composition. Also to note, these measurements were done on samples in the dirty limit ($l < \xi_0$) when $\Delta_g(0)/k_B T_c$ is depressed for single-band materials with anisotropic superconducting order parameters [59]. For NbN, values between 2.04 [60] and 2.12 [61] were reported. The spread in the value of $\alpha = \Delta_g(0)/k_B T_c$ can be related to the sample stoichiometry, more specifically, to the amount of nitrogen incorporated in the crystalline structure. The increase of the concentration of light nitrogen ions leads to an increase of the phonon frequencies and T_c [62]. Changes in the ratio T_c/ω_{ln} could affect the measured α/α_{BCS} ratios according to the strong-coupling corrections [63], which predict that $\frac{\Delta(0)}{k_B T_c} = \alpha_{BCS}\left[1 + 12.5\left(\frac{T_c}{\omega_{ln}}\right)^2 \ln\left(\frac{\omega_{ln}}{2T_c}\right)\right]$, where ω_{ln} is the characteristic phonon frequency [62].

We also performed heat capacitance measurements at various applied magnetic fields up to 9 T. A similar analysis found that the applied field does not significantly change γ_n and θ_D, as seen in Table 1.

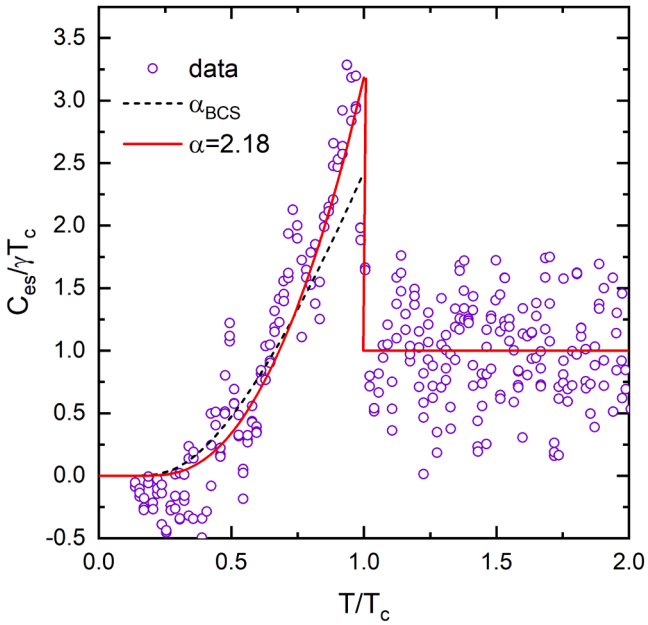

Fig. 3. Temperature dependence of the normalized superconducting heat capacity and the curves obtained with the α-model. The continuous curve is for $\alpha = 2.18$ and the dashed one is for $\alpha_{BCS} = 1.764$ (BCS model).

3.2. AC magnetic susceptibility

AC susceptibility was measured at two static fields of 0.025 T and 0.5 T and amplitudes of the alternative field spanning from 0.1 to 0.9 mT at frequencies between 11 Hz and 10 kHz. Fig. 4(a) shows the temperature dependence of both in-phase χ' and out-of-phase χ'' components of the AC susceptibility as measured at a frequency of 332 Hz for a static field $\mu_0 H = 0.025$ T. Data taken for $\mu_0 H = 0.5$ T are similar except that they are shifted 0.2 K toward lower temperatures. We focused here on measurements at 332 Hz as the dissipation at high AC-amplitude and

Table 1
Data on the field dependence of T_c and normal state as extracted from heat capacity measurements for a $(Nb_{0.63}Ti_{0.37})_{0.50}N_{0.50}$ thick film.

B (T)	T_c (K)	γ_n (mJ/mol/K^2)	β_n (mJ/mol/K^4)	θ_D (K)
0	14.8	2.72±0.24	0.047	345.1
1	14.6	2.0 ± 0.32	0.049	341.0
3	14.3	2.41±0.25	0.048	343.1
5	13.3	1.94±0.23	0.048	344.0
7	12.1	1.72±0.24	0.048	343.8
9	11.2	1.89±0.22	0.048	344.6

frequencies above 1 kHz is significant and led to errors in the temperature reading since the temperature sensor is not mounted on the sample. In addition, relaxation is smaller than at the lowest frequencies. As seen from Fig. 4(a), there is one predominant peak of χ", supporting the idea of a single superconducting phase. The peak is also very slightly dependent on frequency. The temperature T_p of the peak of χ" provides the temperature dependence of J_c (T_p) = h_a/d, where h_a is the amplitude of the AC-field and d is the thickness of the sample. Fig. 4(b) shows the dependence of J_c as obtained from susceptibility data as a function of reduced temperature $t = 1\text{-}(T/T_c)^2$. In the restricted shown temperature range, $J_c = J_{c0}(B)[1\text{-}(T/T_c)^2]^{2.6}$ for both fields. The continuous lines are fits with power low dependence $J_c = J_{c0}t^{\alpha}$.

The real part of the AC susceptibility χ' was used to determine the upper critical field B_{c2} [64] using a frequency of 32 Hz and a field amplitude $\mu_0 h_a = 0.1$ mT. Fig. 5 shows the temperature dependence of B_{c2} (phase diagram) as extracted from heat capacity (circles) and AC-susceptibility (triangles) measurements, respectively. There are discrepancies between the two dependencies, likely because the magnetic measurements are more sensitive to defects and surface effects [65] compared to thermal measurements, which probe the superconducting volume which vanishes at the upper critical field value. Here we use B_{c2} obtained from the heat capacity measurements to estimate the zero temperature Ginzburg-Landau coherence length $\xi(0)$ according to the formula $\xi(0) = \sqrt{\frac{\Phi_0}{2\pi}\left(T_c|\frac{dB_{c2}}{dT}|_{T_c}\right)^{-1}}$. Parameters extracted from heat capacity measurements yield $\xi(0) = 2.55$ nm. Literature reports a tendency of decreasing $\xi(0)$ with increasing the film thickness, with a somewhat weaker dependence on composition. Thus, $\xi(0)$ has values between 5.3.and 6.47 nm (depending on composition) for a 10 nm thick film [66–68] (but also 4.6 and 4.9 nm for similar thickness [69]), 4.65 and 4.35 nm for a thickness of 15 and 20 nm, respectively [36], and 3.8 nm for a film of 500 nm [70]. Accordingly, our films are consistent with a 3D superconductor because the thickness $d >> \xi(0)$.

3.3. DC magnetic susceptibility

The field H dependence of the magnetization M is shown in Fig. 6(a) for temperatures between 5 and 15 K. M was corrected for the diamagnetic contribution of the substrate using magnetization data at $T > T_c$ [see the Inset to Fig. 6(a)].

One observable feature of the hysteresis is the asymmetry between the flux entry and flux exit magnetization. In bulk superconductors, such an asymmetry was observed before and discussed by Gokhfeld et al. [71] based on the extended critical state model [72] using an induction B-dependent J_c. In the case of films, the application of the model is complicated by demagnetization effects, which amplify the applied field at the edges of the film and generate an important curvature of H. As a result, the flux penetration depends nonlinearly on the applied field [73]. Further progress towards understanding asymmetric hysteresis used edge barriers and B-dependent critical current [74]. Since the above-discussed models use an induction dependent critical current density $J_c(B)$, which complicates the evaluation of the applied field dependence of the critical current density, we use the critical state approximation (Bean relationship) [75] for a *qualitative* evaluation of $J_c(H)$:

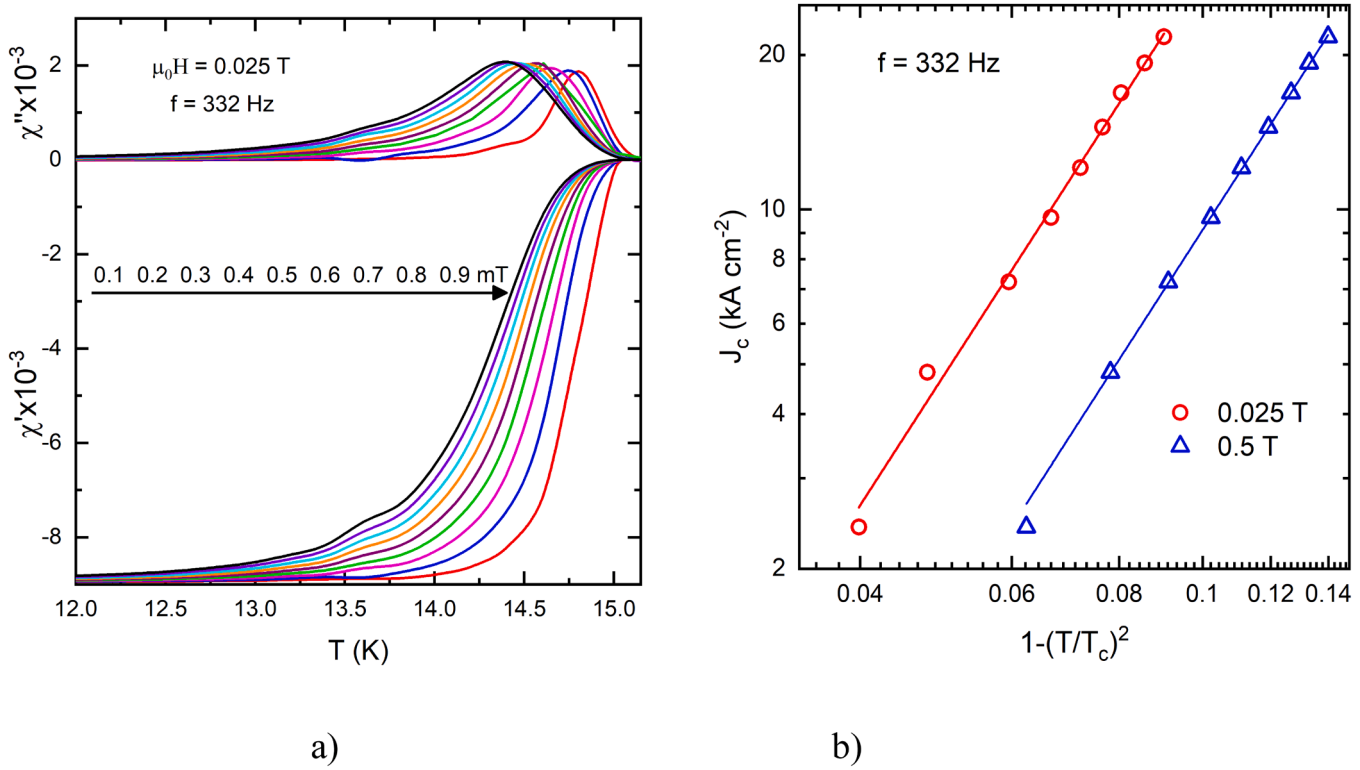

Fig. 4. a) Temperature dependence of the real χ'and the imaginary χ" parts of the AC susceptibility as measured at a constant field of 0.025 T and a frequency of 332 Hz for amplitudes of the alternating field between 0.1 and 0.9 mT. b) Critical current dependence on the reduced temperature $t = 1\text{-}(T/T_c)^2$.

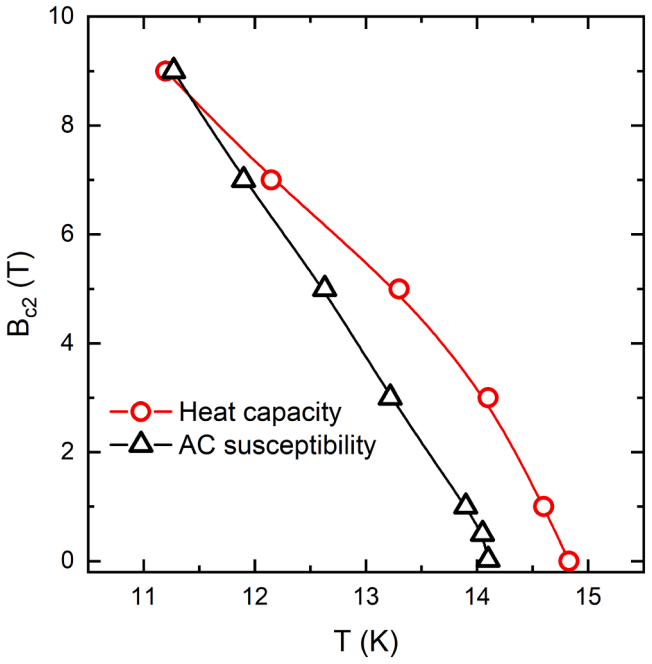

Fig. 5. Field-temperature phase diagram as obtained from heat capacity and AC susceptibility data as measured at 32 Hz and 0.1 mT AC-field amplitude.

$$J_c = \frac{20(M^+ - M^-)}{a(1 - a/3b)} \quad (2)$$

Here, M^- and M^+ are the magnetization on sweeping fields up and down, and $a = b = 0.28$ cm are sample sizes perpendicular to the applied field. After a rather fast decrease at low fields ($\mu_0 H < 3$ T at 5 K, and this limit shifts to lower fields at higher temperatures), the decrease of J_c follows an exponential law at higher field with a T-dependent exponent $J_c \propto \exp[-\zeta(T)B]$. The observed exponent is small, $\zeta < 1$ T^{-1} for $5 < T < 9$ K, but increases rapidly temperatures, $\zeta(11\text{K}) = 2.06$ T^{-1} and $\zeta(13\text{K}) = 3.6$ T^{-1}, as seen in Fig. 6(b).

3.4. Magnetic relaxation

The features of the relaxation are important for the vortex dynamics in superconducting systems as they depict the resilience of NbTiN to fluctuations. Specifically, relaxation becomes important for applications that use persistent currents of high intensity. The strength of thermal fluctuations is quantified by the Ginzburg number $Gi = \frac{1}{2}\left[\frac{\mu_0 k_B T_c}{4\pi B_c(0)^2 \xi^3}\right]^2$ [76]. In the case of NbTiN, $Gi = 10^{-6}$ when using parameters from Ref. 70 and our values for the coherence length. For comparison, this is two orders of magnitude higher than for NbTi ($Gi \sim 10^{-8}$) [77], but much lower than for high-Tc superconductors ($Gi \sim 10^{-2}$) [76].

The time t dependence of the total magnetic moment m=MV was measured on the flux enter branch with the magnet in the persistent mode. Here V is the estimated volume of the film. Magnetic relaxation measurements were performed at $\mu_0 H = 0.25$, 0.5, and 0.75 T. The first data points were taken 100 s after charging the magnet for each applied field and temperature. The dependences of $\ln|m|$ on $\ln(t)$ for the three fields as measured at 8, 10, and 12 K are shown in Fig. 7(a). All data display a logarithmic decay at all temperatures and fields according to Anderson-Kim model [78]. Usually, such a dependence is characterized by a relaxation rate S and by an effective creep activation energy U^* which are defined below [79]:

$$S = -\frac{d\ln(m)}{d\ln(t)} = \frac{k_B T}{U^*} \quad (3)$$

The temperature dependence of the relaxation rates S for the three applied fields H is shown in the Fig. 7(b), whereas the inset to Fig. 7(b) shows the temperature dependence of the effective creep activation energy. The values of S are larger than the universal minimum for the creep rate at a given temperature T, set by $S \sim G_i^{1/2} T/T_c$, below which relaxation cannot be reduced [80]. At low temperatures, S slowly increases with increasing temperature, more conspicuously observed at

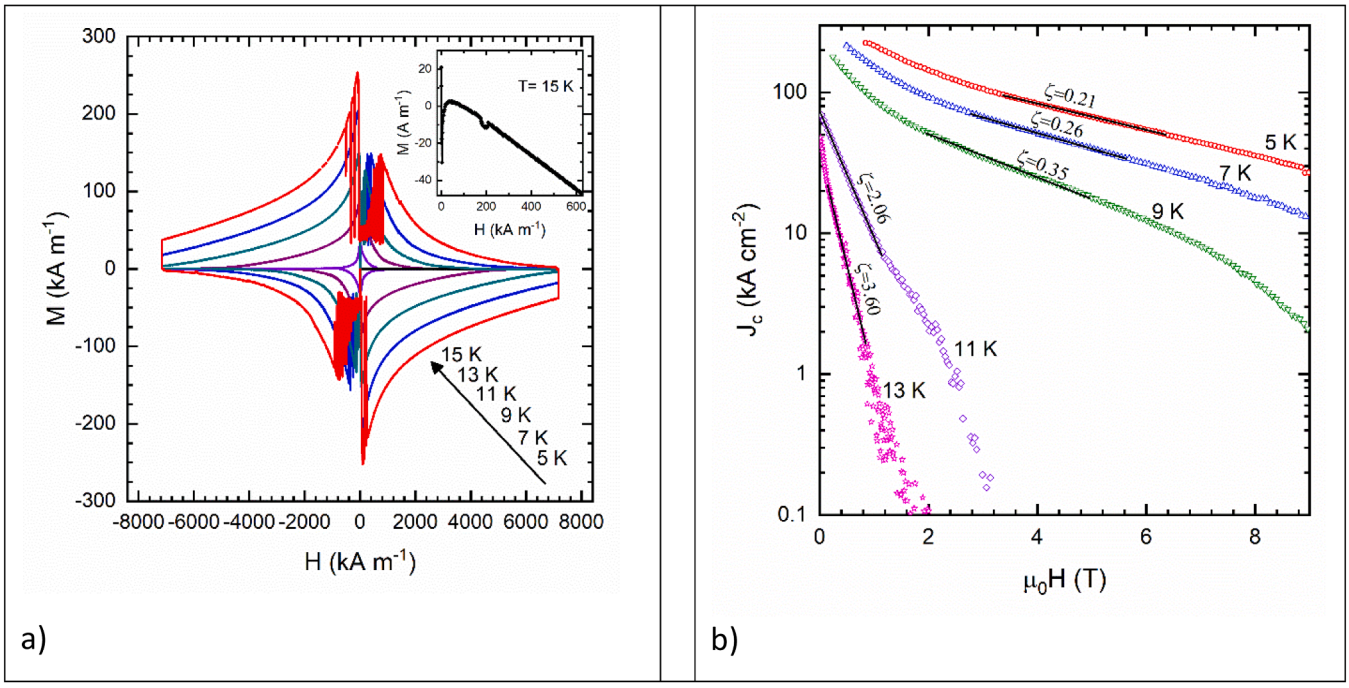

Fig. 6. a). Field dependence of the magnetization for a $(Nb_{0.63}Ti_{0.37})_{0.50}N_{0.50}$ thick film as measured in the temperature range 5-to-15 K. Inset: data taken at $T = T_c$. b) Field dependence of the critical current density. Continuous lines (black) overlaid on measured data are fits with the exponential dependence at intermediate field strength.

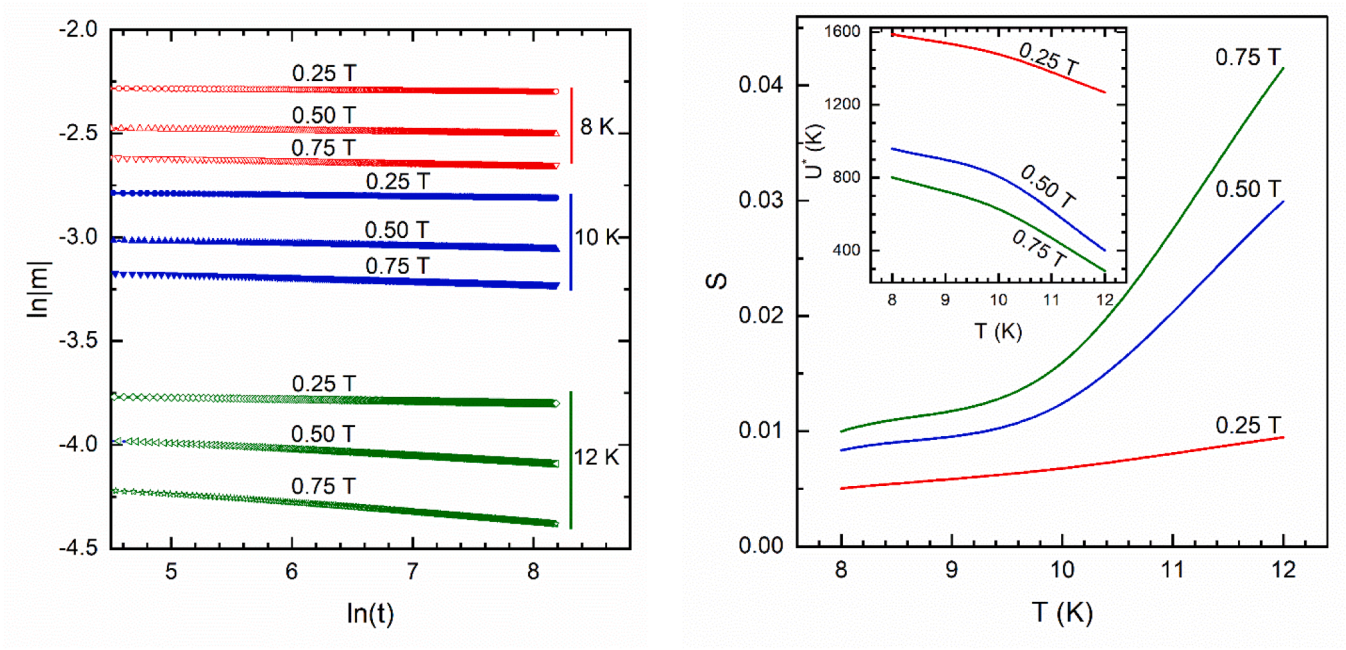

Fig. 7. a). Time decay of the remnant magnetization ln|m| vs. ln(t)(with t in seconds) for $\mu_0 H = 0.25$ T, 0.5 T, and 0.75 T as measured at 8 K, 10 K, and 12 K. b) Temperature dependence of the relaxation rate S as obtained from the relaxation data. Inset: The temperature dependence of the effective creep activation energy U.*

the lowest field, which is consistent with the Anderson-Kim model (weak variation of U^*). An extrapolation to zero does not suggest a zero relaxation, a fact that we attribute to the important role of the electromagnetic noise at low temperatures [81]. At higher fields, there is a sharp increase of the relaxation rate at higher temperatures. This might be explained by the increase of the density of vortices whereas the density of pinning sites remains constant.

The decrease of U^* with field and temperature is the result of a several factors as it depends on temperature T, field H, and current density J [82]. The high values of U^*, the two-dimensionality of the material, and the rather long magnetic penetration length [70] are favorable to the activation of almost rigid vortices (Anderson-Kim regime). However, more investigations would be necessary to establish the regimes of the creep in NbTiN films.

4. Conclusions

In summary, we measured the heat capacity and the magnetic properties of deposited NbTiN films and determined the key electronic, phononic, and superconducting parameters characterizing this material. We found that the zero-temperature coherence length was much smaller than the film thickness, therefore, these results correspond to the bulk limit of NbTiN. This is important as the synthesis of NbTiN in the bulk or single crystal form remains to be reported.

We found that the normalized jump of heat capacity at T_c is larger than the theoretical value proposed for weak coupling BCS superconductors and suggests an extremely strong coupling regime for NbTiN. The B_{c2} values as determined from magnetic measurements are smaller compared to the values extracted from the heat capacity, which brings to light the effect of the defects on B_{c2}. The H-dependence of the DC magnetization was used to determine the field dependence of the critical current density J_c, while the AC susceptibility measurements provided information on the temperature dependence of J_c. However, the temperature range in which the latter quantity was measured was restricted due to the very small separation of the peaks of χ''. Magnetic relaxation measurements found that the effective creep activation energy was rather high, suggesting a Kim-Anderson dependence with rigid vortices excited above energetic barriers. However, the latter assumption needs more investigations.

CRediT authorship contribution statement

Elena Cimpoiasu: Writing – review & editing, Writing – original draft, Investigation, Conceptualization. **Viorel Sandu:** Writing – original draft, Formal analysis, Data curation, Conceptualization. **Karwan Rostem:** Writing – review & editing, Investigation, Conceptualization. **Edward J. Wollack:** Writing – review & editing, Investigation, Funding acquisition, Conceptualization. **Ari D. Brown:** Writing – review & editing, Investigation, Conceptualization. **Kevin H. Miller:** Writing – review & editing, Investigation, Conceptualization. **Vilem Mikula:** Writing – review & editing, Investigation, Conceptualization.

Declaration of competing interest

The authors declare that they have no known competing financial interests or personal relationships that could have appeared to influence the work reported in this paper.

Acknowledgments

This research was supported by the National Aeronautics and Space Administration (NASA) under SOFIA award 15-S3GSI15–2–0003 for development of the HIRMES instrument and Goddard Space Flight Center (GSFC) Internal Research and Development (IRAD) program. The authors gratefully acknowledge S. H. Moseley, A. M. Datesman, and A. Klassen for related discussions and technical support. The views expressed in this article are those of the author and do not reflect the official policy or position of the U.S. Naval Academy, Department of the Navy, the Department of Defense, or the U.S. Government.

Data availability

Data will be made available on request.

References

[1] M.G. Tanner, et al., Enhanced telecom wavelength single-photon detection with NbTiN superconducting nanowires on oxidized silicon, Appl. Phys. Lett. 96 (2010) 221109, https://doi.org/10.1063/1.3428960.

[2] S. Miki, T. Yamashita, H. Terai, Z. Wang, High performance fiber-coupled NbTiN superconducting nanowire single photon detectors with Gifford-McMahon cryocooler, Opt. Express 21 (2013) 10208, https://doi.org/10.1364/OE.21.010208.

[3] C. Schuck, W.H. Pernice, H.X. Tang, Waveguide integrated low noise NbTiN nanowire single-photon detectors with milli-Hz dark count rate, Sci. Rep. 3 (2013) 1893, https://doi.org/10.1038/srep01893.

[4] S.J. Chen, L.X. You, W.J. Zhang, X.Y. Yang, H. Li, L. Zhang, Z. Wang, X.M. Xie, Dark counts of superconducting nanowire single-photon detector under illumination, Opt. Express 23 (2015) 010786, https://doi.org/10.1364/OE.23.010786.

[5] J. Zichi, J. Chang, S. Steinhauer, K. Von Fieandt, J.W.N. Los, G. Visser, N. Kalhor, T. Lettner, A.W. Elshaari, I.E. Zadeh, V. Zwiller, Optimizing the stoichiometry of ultrathin NbTiN films for high-performance superconducting nanowire single-photon detectors, Optics Express 27 (2019) 26579, https://doi.org/10.1364/OE.27.026579.

[6] S. Steinhauer, L. Yang, S. Gyger, T. Lettner, C. Errando-Herranz, K.D. Jöns, M. A. Baghban, K. Gallo, J. Zichi, V. Zwiller, NbTiN thin films for superconducting photon detectors on photonic and two-dimensional materials, Appl. Phys. Lett. 116 (2020) 171101, https://doi.org/10.1063/1.5143986.

[7] J.W. Kooi, J.A. Stern, G. Chattopadhyay, H.G. LeDuc, B. Bumble, J. Zmuidzinas, Low-Loss NbTiN Films for THz SIS Mixer Tuning Circuits, Int. J. Infrared Millimeter Waves 19 (1998) 373, https://doi.org/10.1023/A:1022595223782.

[8] B. Bumble, H. LeDuc, J. Stern, K. Megerian, Fabrication of Nb/Al-N/sub x//NbTiN junctions for SIS mixer applications, IEEE Trans. Appl. Supercond. 11 (2001) 76, https://doi.org/10.1109/77.919288.

[9] B.D. Jackson, A.M. Baryshev, G. de Lange, J.-R. Gao, S.V. Shitov, N.N. Iosad, T. M. Klapwijk, Low-noise 1 THz superconductor–insulator–superconductor mixer incorporating a NbTiN/SiO2/Al tuning circuit, Appl. Phys. Lett. 79 (2001) 436, https://doi.org/10.1063/1.1384005.

[10] L. Jiang, et al., Development of 1.5 THz waveguide NbTiN superconducting hot electron bolometer mixers, Supercond. Sci. Technol. 23 (2010) 045025, https://doi.org/10.1088/0953-2048/23/4/045025.

[11] M.P. Westig, S. Selig, K. Jacobs, T.M. Klapwijk, C.E. Honingh, Improved Nb SIS devices for heterodyne mixers between 700 GHz and 1.3 THz with NbTiN transmission lines using a normal metal energy relaxation layer, J. Appl. Phys. 114 (2013) 124504, https://doi.org/10.1063/1.4822167.

[12] T.M. Miller, A.D. Brown, N. Costen, et al., A Path to High-Efficiency Optical Coupling for HIRMES, J. Low Temp. Phys. 193 (2018) 681–686, https://doi.org/10.1007/s10909-018-1939-7.

[13] P. Fabbricatore, G. Gemme, R. Musenich, R. Parodi, M. Viviani, B. Zhang, V. Buscaglia, Niobium and niobium-titanium nitrides for RF applications, IEEE Trans. Appl. Supercond. 3 (1993) 1761, https://doi.org/10.1109/77.233593.

[14] P. Bosland, S. Cantacuzene, J. Gobin, M. Juillard, J. Martignac, NbTiN thin films for RF applications, in: Proceedings of the 6thWorkshop on RF Superconductivity, CEBAF, Newport News, Virginia, 1993, p. 1028.

[15] C. Benvenuti, P. Chiggiato, L. Parrini, R. Russo, Production of niobium-titanium nitride coatings by reactive diffusion for superconducting cavity applications, Nucl. Instrum. Methods Phys. Res., Sect. B 124 (1997) 106, https://doi.org/10.1016/S0168-583X(97)00059-1.

[16] A. Endo, C. Sfiligoj, S.J.C. Yates, J.J.A. Baselmans, D.J. Thoen, S.M.H. Javadzadeh, P.P. van der Werf, A.M. Baryshev, T.M. Klapwijk, On-chip filter bank spectroscopy at 600–700 GHz using NbTiN superconducting resonators, Appl. Phys. Lett. 103 (2013) 032601, https://doi.org/10.1063/1.4813599.

[17] T. Hong, K. Choi, K.I. Sim, T. Ha, B.C. Park, H. Yamamori, J.H. Kim, Terahertz electrodynamics and superconducting energy gap of NbTiN, J. Appl. Phys. 114 (2013) 243905, https://doi.org/10.1063/1.4856995.

[18] M.C. Burton, M.R. Beebe. K. Yang. R. A. Lukaszew, A.-M. Valente-Feliciano. C. Reece, Superconducting NbTiN thin films for superconducting radio frequency accelerator cavity applications, J. Vac. Sci. Technol. A 34 (2016) 021518, https://doi.org/10.1116/1.4941735.

[19] Md Tohidul Islam, Q. Liu, S. Broderick, Machine Learning Accelerated Design of High-Temperature Ternary and Quaternary Nitride Superconductors, Appl. Sci. 14 (2024) 9196, https://doi.org/10.3390/app14209196.

[20] I.E. Zadeh, et al., Efficient Single-Photon Detection with 7.7 ps Time Resolution for Photon-Correlation Measurements, ACS Photonics 7 (2020) 1780, https://doi.org/10.1021/acsphotonics.0c00433.

[21] J.W. Niels Los, et al., High-performance photon number resolving detectors for 850–950 nm wavelength range, APL Photonics 9 (2024) 066101, https://doi.org/10.1063/5.0204340.

[22] J. Chang, J.W. Los, J.O. Tenorio-Pearl, N. Noordzij, R. Gourgues, A. Guardiani, J. R. Zichi, S.F. Pereira, H.P. Urbach, V. Zwiller, S.N. Dorenbos, I.E. Zadeh, et al., Detecting telecom single photons with (99.5-2.06+0.5) % system detection efficiency and high time resolution, APL Photonics 6 (2021) 036114.

[23] D.V. Reddy, R.R. Nerem, S.W. Nam, R.P. Mirin, V.B. Verma, Superconducting nanowire single-photon detectors with 98% system detection efficiency at 1550 nm, Optica 7 (2020) 1649.

[24] X. Yang, L. You, L. Zhang, C. Lv, H. Li, X. Liu, H. Zhou, Z. Wang, Comparison of Superconducting Nanowire Single-Photon Detectors Made of NbTiN and NbN Thin Films, IEEE Trans. Appl. Supercond. 28 (2018) 22106.

[25] J. Chang, et al., Efficient mid-infrared single-photon detection using superconducting NbTiN nanowires with high time resolution in a Gifford-McMahon cryocooler, Photonics Research 10 (2022) 1063, https://doi.org/10.1364/PRJ.437834.

[26] G.G. Taylor, et al., Mid-infrared timing jitter of superconducting nanowire single-photon detectors, Appl. Phys. Lett. 121 (2022) 214001, https://doi.org/10.1063/5.0128129.

[27] Ruoyan Ma, et al., Single photon detection performance of highly disordered NbTiN thin films, J. Phys. Commun. 7 (2023) 055006, https://doi.org/10.1088/2399-6528/acd747.

[28] D. Zhu, M. Colangelo, C. Chen, B.A. Korzh, F.N.C. Wong, M.D. Shaw, K. K. Berggren, Resolving photon numbers using a superconducting nanowire with impedance-matching taper, Nano Letters 20 (2020) 3858.

[29] J.W.N. Los, M. Sidorova, B. Lopez-Rodriguez, P. Qualm, J. Chang, S. Steinhauer, V. Zwiller, I.E. Zadeh, High-performance photon number resolving detectors for 850–950 nm wavelength range, APL Photonics 9 (2024) 066101.

[30] C. Schuck, W.H.P. Pernice, H.X. Tang, Waveguide integrated low noise NbTiN nanowire single-photon detectors with milli-Hz dark count rate, Sci. Rep. 3 (2013) 1893, https://doi.org/10.1038/srep01893.

[31] G.V. Resta, et al., Gigahertz Detection Rates and Dynamic Photon-Number Resolution with Superconducting Nanowire Arrays, Nano Letters 23 (2023) 6018, https://doi.org/10.1021/acs.nanolett.3c01228.

[32] A. Azem, et al., Mid-infrared charact ts erization of NbTiN superconducting nanowire single-photon detectors on silicon-on-insulator, Appl. Phys. Lett. 125 (2024) 211102, https://doi.org/10.1063/5.0237005.

[33] H. Yamamori, H. Sasaki, S. Kohjiro, Preparation of overdamped NbTiN Josephson junctions with bilayered Ti–TiN barriers, J. Appl. Phys. 108 (2010) 113904, https://doi.org/10.1063/1.3517475.

[34] V.I. Ivashchenko, P.E.A. Turchi, E.I. Olifan, Phase stability and mechanical properties of niobium nitrides, Phys. Rev. B 82 (2010) 054109, https://doi.org/10.1103/PhysRevB.82.054109.

[35] M. Dressel, Electrodynamics of Metallic Superconductors, Adv. Condens. Matter Phys. 2013 (2013) 104379, https://doi.org/10.1155/2013/104379.

[36] A. Yu. Mironov, et al., Charge Berezinskii-Kosterlitz-Thouless transition in superconducting NbTiN films, Sci. *Re.* 8 (2018) 4082, https://doi.org/10.1038/s41598-018-22451-1.

[37] E.F.C. Driessen, P.C.J.J. Coumou, R.R. Tromp, P.J. de Visser, T.M. Klapwijk, Strongly disordered TiN and NbTiN s-wave superconductors probed by microwave electrodynamics, Phys. Rev. Lett. 109 (2012) 107003, https://doi.org/10.1103/PhysRevLett.109.107003.

[38] M.C. Burton, M.R. Beebe, K. Yang, J. Riso, A. Lukaszew, A.M. Valente-Feliciano, C. E. Reece, Superconducting NbN-based multilayer and NbTiN thin films for the enhancement of SRF accelerator cavities, in: Proc. SRF, Whistler, BC, Canada, 2015, p. 638, https://doi.org/10.18429/JACoW-SRF2015-TUPB037. Eds. R. E. Laxdal, J. Thomson, V. R. W Schaa. ISBN 978-3-95450-178-6.

[39] M. Sidorova, A.D. Semenov, H.-W. Hübers, S. Gyger, S. Steinhauer, Phonon heat capacity and self-heating normal domains in NbTiN nanostrips, Supercond. Sci. Technol. 35 (2022) 105005, https://doi.org/10.1088/1361-6668/ac8454.

[40] K. Makise, H. Terai, M. Takeda, Y. Uzawa, Z. Wang, Characterization of NbTiN Thin Films Deposited on Various Substrates, IEEE Trans. Appl. Supercond. 21 (2011) 139, https://doi.org/10.1109/TAS.

[41] L. Zhang, W. Peng, L.X. You, Z. Wang, Superconducting properties and chemical composition of NbTiN thin films with different thickness, Appl. Phys. Lett. 107 (12) (2015) 122603, https://doi.org/10.1063/1.4931943.

[42] H. Myoren, T. Shimizu, T. Iiziika, S. Takada, Properties of NbTiN Thin Films Prepared by Reactive DC Magnetron Sputtering, IEEE Trans. Appl. Supercond. 11 (2001) 3828, https://doi.org/10.1109/77.919899.

[43] G.R. Stewart, Heat Capacity of Superconducting Materials, in: R.R. Reed, A.F. Clark (Eds.), Advances in Cryogenic Engineering Materials, Advances in Cryogenic Engineering Materials, 32, Springer, Boston, MA, 1986, https://doi.org/10.1007/978-1-4613-9871-4_101, 1986.

[44] H.-H. Wen, Specific heat in superconductors, Chinese Phys. B 29 (2020) 017401, https://doi.org/10.1088/1674-1056/ab5a3d.

[45] J.P. Carbotte, Properties of boson-exchange superconductors, Rev. Mod. Phys. 62 (1990) 1027.

[46] E.S.R. Gopal, Specific Heats at Low Temperatures. The International Cryogenics Monograph Series. K. Mendelssohn and K. D. Timmerhaus Editors, Plenum Press New York, 1966, https://doi.org/10.1007/978-1-4684-9081-7. ISBN 978-1-4684-9083-1, ISBN 978-1-4684-9081-7 (eBook).

[47] M. Sidorova, A.D. Semenov, H.-W. Hübers, et al., Magnetoconductance and photoresponse properties of disordered NbTiN films, Phys. Rev. B 104 (2021) 184514, https://doi.org/10.1103/PhysRevB.104.184514.

[48] X. Lang, Q. Jiang, Finite size effect on critical transition temperature of superconductive nanosolids, Solid State Commun 134 (2005) 797, https://doi.org/10.1016/j.ssc.2005.03.039.

[49] W. Frick, D. Waldmann, W. Eisenmenger, Phonon emission spectra of thin metallic films, Appl. Phys. 8 (1975) 163, https://doi.org/10.1007/BF00896033.

[50] A. Zaccone, Quantum confinement theory of the heat capacity of thin films, Phys. Rev. Materials 8 (2024) 056001, https://doi.org/10.1103/PhysRevMaterials.8.056001.

[51] S. Chong, J.-Q. Shen, Even–Odd Layer Oscillatory Behavior of Electronic and Phononic Specific Heat in an Ultra-Thin Metal Film, Materials 17 (19) (2024) 4851, https://doi.org/10.3390/ma17194851.
[52] W. Ma, X. Zhang, K. Takahashi, Electrical properties and reduced Debye temperature of polycrystalline thin gold films, J. Phys. D: Appl. Phys. 43 (2010) 465301, https://doi.org/10.1088/0022-3727/43/46/465301.
[53] M.M. Arockiasamy, M. Sundareswari, M. Rajagopalan, Ductility behavior of cubic titanium niobium nitride ternary alloy: a first-principles study, Indian J. Phys. 9 (2016) 149, https://doi.org/10.1007/s12648-015-0736-2.
[54] M.N. Khlopkin, The specific heat of Nb_3Sn in magnetic fields up to 19 T, Sov. Phys. JETP 63 (1986) 164.
[55] D.C. Johnston, Elaboration of the α-model derived from the BCS theory of superconductivity, Supercond. Sci. Technol. 26 (2013) 115011, https://doi.org/10.1088/0953-2048/26/11/115011.
[56] T. Hong, K. Choi, K. Ik Sim, T. Ha, B.C. Park, H. Yamamori, J.H. Kim, Terahertz electrodynamics and superconducting energy gap of NbTiN, J. Appl. Phys. 114 (2013) 243905, https://doi.org/10.1063/1.4856995.
[57] A. Khudchenko, et al., Dispersive Spectrometry at Terahertz Frequencies for Probing the Quality of NbTiN Superconducting Films, IEEE Trans. Appl. Supercond. 32 (2022) 1500506, https://doi.org/10.1109/TASC.2022.3147736.
[58] N.R. Groll, et al., Tunneling spectroscopy of superconducting MoN and NbTiN grownby atomic layer deposition, Appl. Phys. Lett. 104 (2014) 092602, https://doi.org/10.1063/1.4867880.
[59] L.A. Openov, Effect of nonmagnetic and magnetic impurities on the specific heat jump in anisotropic superconductors, Phys. Rev. B 69 (2004) 224516, https://doi.org/10.1103/PhysRevB.69.224516.
[60] K. Komenou, T. Yamashita, Y. Onodera, Energy gap measurement of niobium nitride, Phys. Lett. A 28 (1968) 335–336, https://doi.org/10.1016/0375-9601(68)90319-8.
[61] Y.F. Wu, A.B. Yu, L.B. Lei, et al., Superconducting NbN and $CaFe_{0.88}Co_{0.12}AsF$ studied by point-contact spectroscopy with a nanoparticle Au array, Phys. Rev. B. 101 (2020) 174502, https://doi.org/10.1103/PhysRevB.101.174502.
[62] B.P. Allen, R.C. Dynes, Transition temperature of strong-coupled superconductors reanalyzed, Phys. Rev. B 12 (1975) 905, https://doi.org/10.1103/PhysRevB.12.905.
[63] B. Mitrovic, H.G. Zarate, J.P. Carbotte, The ratio $2\Delta_0/kBTc$ within Eliashberg theory, Phys. Rev. B 29 (1984) 184, https://doi.org/10.1103/PhysRevB.29.184.
[64] K.-H. Müller, G. Fuchs, A. Handstein, K. Nenkov, V.N. Narozhnyi, D. Eckert, The upper critical field in superconducting MgB_2, J. Alloys Compounds 322 (2001) L10–L13, https://doi.org/10.1016/S0925-8388(01)01197-5.
[65] V. Kozhevnikov, A.-M. Valente-Feliciano, P.J. Curran, A. Sutter, A.H. Liu, G. Richter, E. Morenzoni, S.J. Bending, C. Van Haesendonck, Equilibrium properties of superconducting niobium at high magnetic fields: a possible existence of a filamentary state in type-II superconductors, Phys. Rev. B 95 (2017) 174509.].
[66] D. Hazra, et al., Superconducting properties of NbTiN thin films deposited by high-temperature chemical vapor deposition, Phys. Rev. B 97 (2018) 144518, https://doi.org/10.1103/PhysRevB.97.144518.
[67] M. Jönsson, R. Vedin, S. Gyger, et al., Current Crowding in Nanoscale Superconductors within the Ginzburg-Landau Model, Phys. Rev. Appl. 17 (2022) 064046, https://doi.org/10.1103/PhysRevApplied.17.064046.
[68] M. Nazir, X. Yang, H. Tian, et al., Investigation of dimensionality in superconducting NbN thin film samples with different thicknesses and NbTiN meander nanowire samples by measuring the upper critical field, Chinese Phys. B 29 (2020) 087401, https://doi.org/10.1088/1674-1056/ab9740.
[69] M. Sidorova, A.D. Semenov, H.W. Hübers, et al., Magnetoconductance and Photoresponse Properties of Disordered NbTiN Films, Phys. Rev. B 104 (2021) 184514, https://doi.org/10.1103/PhysRevB.104.184514.
[70] Y. Lee, J. Yun, C. Lee, M. Sirena, J. Kim, N. Haberkorn, Penetration depth in dirty superconducting NbTiN thin films grown at room temperature, Appl. Phys. A 130 (2024) 504, https://doi.org/10.1007/s00339-024-07650-0.
[71] D.M. Gokhfeld, D.A. Balaev, M.I. Petrov, S.I. Popkov, K.A. Shaykhutdinov, V. V, Val'kov, Magnetization asymmetry of type-II superconductors in high magnetic fields, J. Appl. Phys. 109 (2011) 033904, https://doi.org/10.1063/1.3544038.
[72] D.-X. Chen, R.W. Cross, A. Sanchez, Cryogenics 33 (1993) 695, https://doi.org/10.1016/0011-2275(93)90022-G.
[73] E. Zeldov, J.R. Clem, M. McElfresh, M. Darwin, Magnetization and transport currents in thin superconducting films, Phys. Rev. B 49 (1994) 9802, https://doi.org/10.1103/PhysRevB.49.9802.
[74] I.L. Maksimova, D. Yu.Vodolazov, I.L. Maksimov, Magnetization curves and ac susceptibilities in type-II superconductors, geometry-independent similarity and effect of irreversibility mechanisms, Physica C 356 (2001) 67, https://doi.org/10.1016/S0921-4534(01)00090-9.
[75] C.P. Bean, Magnetization of High-Field Superconductors, Rev. Mod. Phys. 36 (1964) 31, https://doi.org/10.1103/RevModPhys.36.31.
[76] G. Blatter, M.V. Feigel'man, V.B. Geshkenbein, A.I. Larkin, V.M. Vinokur, Vortices in the high-temperature superconductors, Rev. Mod. Phys. 66 (1994) 1125.
[77] Y. Lee, J. Yun, C. Lee, M. Sirena, J. Kim, N. Haberkorn, Phys. Scr. 99 (2024) 065963, https://doi.org/10.1088/1402-4896/ad4690.
[78] P.W. Anderson, Y.B. Kim, Hard Superconductivity: theory of the Motion of Abrikosov Flux Lines, Rev. Mod. Phys. 36 (1964) 39, https://doi.org/10.1103/RevModPhys.36.39.
[79] Y. Yeshurun, A.P. Malozemoff, A. Shaulov, Magnetic relaxation in high-temperature superconductors, Rev. Mod. Phys. 68 (1996) 911, https://doi.org/10.1103/RevModPhys.68.911.
[80] N.Miura Eley, B. Maiorov, et al., Universal lower limit on vortex creep in superconductors, Nature Mater 16 (2017) 409–413, https://doi.org/10.1038/nmat4840.
[81] A.N. Lykov, On the possibility of explaining the high rate of flux creep at ultra-low temperatures using the Anderson model, Supercond. Sci. Technol. 26 (2013) 055023, https://doi.org/10.1088/0953-2048/26/5/055023.
[82] L. Miu, I. Ivan, G. Aldica, P. Badica, J.R. Groza, D. Miu, G. Jakob, H. Adrian, Analysis of magnetization relaxation in MgB_2 bulk samples obtained by electric-field assisted sintering, Physica C 468 (2008) 2279–2282, https://doi.org/10.1016/j.physc.2008.08.001.